Monthly Notices of the ROYAL ASTRONOMICAL SOCIETY

MNRAS **502,** 5658–5667 (2021) doi:10.1093/mnras/stab462
Advance Access publication 2021 February 17

Synchronized periodic maser flares of multiple OH and CH_3OH lines in G323.459–0.079

G. C. MacLeod,[1,2]★ Derck P. Smits ,[3]★ J. A. Green[4] and S. P. van den Heever[2]

[1]*Department of Physics and Astronomy, The University of Western Ontario, 1151 Richmond Street, London, ON N6A 3K7, Canada*
[2]*Hartebeesthoek Radio Astronomy Observatory, PO Box 443, Krugersdorp 1741, South Africa*
[3]*Department of Mathematical Sciences, University of South Africa, Private Bag X6, Florida 1709, South Africa*
[4]*CSIRO Astronomy and Space Science, 26 Dick Perry Avenue, Kensington, WA 6151, Australia*

Accepted 2021 February 12. Received 2021 February 9; in original form 2021 January 16

ABSTRACT

The first confirmed periodically varying 6.031 and 6.035 GHz hydroxyl masers are reported here. They vary contemporaneously with the 6.7 GHz methanol masers in G323.459–0.079. The 1.665 GHz hydroxyl and 12.2 GHz methanol masers associated with G323.459–0.079 are also periodic. Evidence for periodicity is seen in all features in all transitions save a single 1.665 GHz hydroxyl maser feature. Historical excited-state hydroxyl maser observations set a stricter upper limit on the epoch in which a significant accretion event occurred. The associated burst in 6.7 GHz methanol maser activity has subsided significantly while the hydroxyl transitions are brightening possibly the result of changing physical conditions in the masing cloudlets. Time lags in methanol are confirmed and may be the result of the periodic flaring propagating outward from the central region of maser activity. A possible magnetic field reversal occurred during the accretion event.

Key words: masers – stars: formation – stars: protostars – ISM: individual objects: G323.459–0.079 – ISM: molecules – radio lines: ISM.

1 INTRODUCTION

The source that we refer to as G323.459–0.079 (RA = $15^h\,29^m\,19\overset{s}{.}40$, Dec. = $-56^\circ\,31'\,23\overset{''}{.}5$ (J2000)) does not have a unique identity in the SIMBAD database (as of 2020 May), but there are five sources listed within 2 arcsec of this position. The IRAS Point Source Catalog (PSC) identified an H II region, IRAS 15254–5621, near this position based on FIR colour ratios from its photometric measurements. The Midcourse Space Experiment (MSX) and 2MASS PSCs have identified sources close to the position of the IRAS source. Masers of hydroxyl (Caswell & Haynes 1987), water (Caswell et al. 1989), and methanol (Kemball, Gaylard & Nicolson 1988; MacLeod, Gaylard & Nicolson 1992) occur here as well as a compact radio continuum source (Walsh et al. 1998), and there is a source identified as a massive young star-forming region, probably still at an early stage of its development (Mottram et al. 2007). The IR sources, compact radio emission, H II region and masers are all components of star-forming regions and hence it makes sense to combine them all into one object using a generic position for G323.459–0.079 that is within the error bars of all the quoted positions. The proposed distance to G323.459–0.079 given by Green & McClure-Griffiths (2011) which provides the best fit to observations is the near kinematic distance at $D = 3.8 \pm 0.4$ kpc.

A more detailed discussion of the maser discoveries in G323.459–0.079 follows. Groundstate OH (hereafter referred to as gsOH) 1.665 GHz masers were first reported by Caswell & Haynes (1987) who noted that the left- and right-circularly polarized (LCP and RCP, respectively) maser lines had peaks at different velocities, suggesting Zeeman splitting due to the presence of magnetic fields of a few milliGauss (mG). Independently, Cohen, Baart & Jonas (1988) detected 1.665 and 1.667 GHz gsOH masers towards the bright far-infrared source IRAS15254–5621. Caswell et al. (1989) detected 22.2 GHz water masers towards this source in 1981. Class II 6.7 and 12.2 GHz methanol masers were discovered by MacLeod et al. (1992) and Kemball et al. (1988), respectively. Maser emission from excited-state OH (hereafter referred to as exOH) at 6.035 GHz was reported by Smits (1994) who found emission in three velocity ranges between $v = [-70.8, -65.5]$ km s^{-1}. Similar results were reported by Caswell & Vaile (1995) from observations made using the Parkes radio telescope in 1993 September and 1994 March. Spectra obtained in 2001 May and September by Caswell (2003) using Parkes led to the discovery of 6.031 GHz exOH masers. (Note this source is listed with a typographical error, G323.459–0.279, in table 1 of Caswell (2003).] These masers had velocities similar to the three groups found for the 6.035 GHz masers. The LCP and RCP components of the 6.031 and 6.035 GHz exOH maser lines had slightly different velocities, consistent with Zeeman splitting of the circular components seen in the gsOH lines. Positions of the 6.035 GHz exOH and 6.7 GHz methanol masers were determined using the Australia Telescope Compact Array (ATCA) from observations done in 1994 May. The ATCA maps show that the methanol and exOH masers were clustered inside the region of radio continuum emission.

The phenomenon of periodicity in masers associated with high mass star-forming regions (HMSFR) was first reported by Goedhart, Gaylard & van der Walt (2003) for 6.7 GHz methanol. Since then another 24 periodic masers associated with HMSFR have been discovered (Goedhart, Gaylard & van der Walt 2004; Goedhart et al.

★ E-mail: gord@hartrao.ac.za (GCM); Derck.Smits@gmail.com (DPS)

Table 1. Spectral transitions observed and receiver packages used at HartRAO. The average root-mean-square (rms) 1σ noise level (and standard deviation in parenthesis) found for the monitoring is presented.

Molecule	Receiver	Maser Transition	Frequency	Beam width	Bandwidth	Velocity Range	Velocity Resolution	Noise Level 1σ rms
	(cm)		(GHz)	(arcmin)	(MHz)	(km s^{-1})	(km s^{-1})	(Jy)
OH	18	$^2\Pi_{J=3/2}\ F=1\rightarrow1$	1.665 402	29.6	0.5	45.0	0.045	2(1)
	5	$^2\Pi_{J=5/2}\ F=2\rightarrow2$	6.030 747	7.5	1.0	24.5	0.049	0.3(1)
	5	$^2\Pi_{J=5/2}\ F=3\rightarrow3$	6.035 092	7.5	1.0	24.5	0.049	0.3(2)
	6	$^2\Pi_{J=1/2}\ F=0\rightarrow1$	4.660 242	9.6	1.0	32.0	0.063	∼0.1
	6	$^2\Pi_{J=1/2}\ F=1\rightarrow0$	4.765562	9.6	1.0	32.0	0.061	0.2(1)
CH_3OH	4.5	$J=5_1\rightarrow6_0\ A^+$	6.668 518	7.0	1.0	22.5	0.044	1.2(3)
	2.5	$J=2_0\rightarrow3_{-1}\ E$	12.178 593	4.0	2.0	24.5	0.048	1.5(6)
H_2O	1.3	$J=6_{16}\rightarrow5_{23}$	22.235 120	2.2	8.0	107.9	0.105	0.6(2)

2009; Araya et al. 2010; Szymczak et al. 2011, 2016; Maswanganye et al. 2015, 2016; Szymczak, Wolak & Bartkiewicz 2015; Sugiyama et al. 2017; Proven-Adzri et al. 2019; Olech et al. 2020). In addition to 6.7 GHz methanol, some sources have contemporaneous periodic 1.665 GHz gsOH (Green et al. 2012b), 4.829 GHz formaldehyde (Araya et al. 2010), and 22.2 GHz water anticorrelated (Szymczak et al. 2016) masers. No periodicity at other transitions, in particular for exOH transitions, have been reported yet. Proven-Adzri et al. (2019) reported eight periodic flares of 6.7 GHz methanol masers in G323.459–0.079 in five different velocity channels.

There are currently three models proposed to explain this periodicity: a pulsating protostellar object (Sanna et al. 2015), a rotating spiral shock (Parfenov & Sobolev 2014), and a colliding wind binary system (van der Walt et al. 2016). To establish which mechanism is responsible for the maser emission periodicity, a larger sample of periodic maser sources, and monitoring at more transitions towards each source, are required to constrain the models.

In this paper, the results of monitoring 1.665, 6.031, and 6.035 GHz OH, 6.7 and 12.2 GHz CH_3OH, and 22.2 GHz H_2O masers associated with G323.459–0.079 using facilities at the Hartebeesthoek Radio Astronomy Observatory (HartRAO) are presented. The first confirmed periodic exOH masers are reported. In fact, observations here show that almost all features detected at 1.665, 6.031, and 6.035 GHz OH, and 12.2 GHz methanol masers vary contemporaneously, and periodically, with the 6.7 GHz methanol masers. Using historical data, limits are placed on the epoch in which a flaring event similar to that seen in NGC 6334I reported by Hunter et al. (2018b) and MacLeod et al. (2018) may have occurred.

2 OBSERVATIONS

Most observations reported here were made using the 26-m telescope of the HartRAO.[1] The 1.3, 2.5, 4.5, 5, 6, and 18 cm receivers are dual RCP and LCP feeds. The handedness of each feed is oriented to conform with conventions set by the International Astronomical Union and the Institute of Electrical and Electronics Engineers (Hamaker & Bregman 1996). It is noted that none of the receivers were calibrated for absolute polarization observations. All front-ends are cryogenically cooled, except for the 2.5-cm receiver which is at ambient temperature. Each polarization was calibrated independently relative to Hydra A and 3C 123 (and Jupiter for the 1.3-cm receiver), assuming the flux scale of Ott et al. (1994). Information pertaining to the transitions observed and receiver packages employed at HartRAO are listed in Table 1.

[1]See http://www.hartrao.ac.za/spectra/ for further information.

Observations were recorded with a 1024-channel per polarization and all employed the method of frequency switching. Half-power beam-width pointing correction observations were made for all epochs of the 1.3, 2.5, and 4.5-cm observations. The beam-width, and bandwidth used for each transition, along with velocity range and resolution are listed in Table 1. Every transition observed was corrected for the Local Standard of Rest (LSR) velocity $v_{\rm LSR} = -67.0$ km s^{-1}.

Historical 5 and 6 cm exOH observations were made in 1994 (Smits 1994) and 1995 (unpublished). The velocity resolution and sensitivity are the same as for the recent observations; however, the total velocity range was half of the current value. For the historical observations linear feeds were used and a circular polarizer placed in front of the feed to obtain LCP and RCP spectra, usually on different days.

From early 2013 to 2015, 5 and 6-cm exOH observations were made at frequencies of 4.660, 4.765, 6.031, and 6.035 GHz but not at 4.750, 6016, or 6.049 GHz. Monitoring of G323.459–0.079 at these frequencies began in 2018 February. Monitoring of the 6.031 GHz emission was carried out after 2019 September when the radio frequency interference (RFI) environment improved markedly. Typically, observations were done every 5–15 d.

To supplement the HartRAO data, spectra of 6.031, 6.035 GHz OH and 6.7 GHz CH_3OH taken between 2011 August 29 and September 2 using the ATCA are included in this paper. The velocity resolutions used for the exOH and methanol observations were 0.024 and 0.022 km s^{-1}, respectively. These spectra were originally published in Green, Caswell & McClure-Griffiths (2015), which provides more details of the observations and data reduction.

3 DATA ANALYSIS

The term 'channel' is used here to specify a specific velocity component in the 512 channels that comprise each spectrum. When the term 'feature' is used it refers to a group of sequential channels that appear to be synchronized emission; these features may be comprised of one or more line-blended masers (components). A central velocity channel is used to identify a given feature. However, there is no spatial information in spectra and a feature here does not refer to a specific maser 'cloudlet' or a distinct gas condensation. At all times every velocity representation is a Local-Standard-of-Rest (LSR) velocity, $v_{\rm LSR}$.

3.1 Creating time series

The simplest time series are created by selecting a single velocity channel in a spectrum and plotting the flux density F versus MJD.

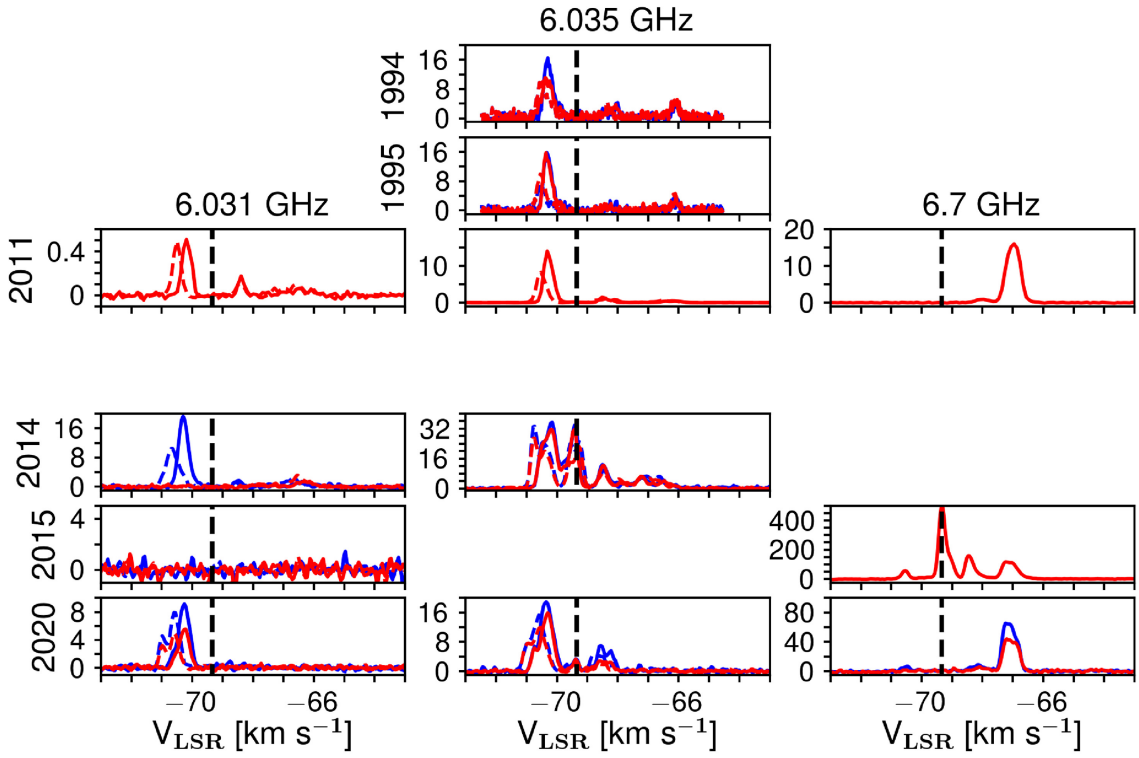

Figure 1. Selected spectra for 6.031 GHz (Column 1), 6.035 GHz exOH (Column 2), and 6.7 GHz CH_3OH (Column 3) masers observed towards G323.459–0.079. The 2011 observations are from the ATCA, all other data are from HartRAO. RCP and LCP spectra are represented by solid and dashed lines, respectively. The black dashed line in each frame indicates the velocity of the strong methanol maser at $v = -69.35\,\mathrm{km\,s^{-1}}$ that appeared in the 2015 spectrum. Blue lines represent observations taken several months before those plotted in red.

However, these data may suffer from RFI or velocity and/or line blending variations. To overcome the RFI, the integrated flux density, F_{Int}, of each feature is determined for each epoch of observation. In rare instances individual spectral channels were used. Around each central velocity channel, a velocity range between 0.5 and $1.0\,\mathrm{km\,s^{-1}}$ is set, preferably larger than the velocity extent of the feature. This extent varied for each feature dependent upon its isolation from other features and the level of RFI in the spectrum. The observing frequency band containing the 1.665 GHz emission (1.585–1.745 GHz) is significantly impacted by sources of RFI, particularly those attributed to satellite based emission, not readily mitigated. In this band, the worst affected epochs were removed. Note that no statistically significant velocity drifts were found in these data.

3.2 Periodicity and time-lag measurements

Two methods were used to determine the periodicity of each maser feature. The first method uses the Lomb–Scargle (LS) periodogram (Scargle 1982) to determine the period, τ_{LS}. The second method measures the time difference between consecutive peaks of flaring features (PP) to determine a period τ_{PP}. The method is described in MacLeod et al. (2020). Time lags between features are determined by comparing the dates of maximum (minimum) to those of the $v = -68.13\,\mathrm{km\,s^{-1}}$ feature. With these time series time lags Δt_{max} and Δt_{min} were determined. If $\Delta t < 0$, then the feature in question reached its maximum (minimum) prior to that of the feature at $v = -68.13\,\mathrm{km\,s^{-1}}$. There are 16 flare cycles presented here which are referred to using labels $n = 1$–16.

4 RESULTS

4.1 Pre-monitoring observations

Prior to the monitoring observations that started in 2018 February, observations towards G323.459–0.079 were made irregularly. Some variation can be seen in the exOH maser lines from one observation epoch to the next, but the observations are too sparse to attribute these changes to periodic variations. No emissions from OH transitions at 4.660 or 4.765 GHz were detected above a level of $3\sigma - 0.5$ Jy at any stage from 1994 up to the present at HartRAO, or was any 22 GHz water emission detected above a level of $3\sigma - 2$ Jy.

In Fig. 1 spectra of the 6.031, 6.035 GHz OH and 6.7 GHz CH_3OH masers in G323.459–0.079 are presented. Interferometric observations from Green et al. (2015) for 6.031 and 6.035 GHz exOH and 6.7 GHz CH_3OH transitions in 2011 are also shown. The bottom panel shows the spectra taken during the phase minimum and maximum of flare 14 in 2020 for comparison purposes.

When the 6.031 GHz OH maser emission was first reported by Caswell (2003) it had a peak flux density $F < 0.6$ Jy with emission over a velocity range of $\Delta v \sim 7\,\mathrm{km\,s^{-1}}$. In 2011, the spectrum was similar, but by 2014 the peak had increased to ∼18 Jy before dropping below detectable levels, $3\sigma - 0.5$ Jy. This state continued through 2015. When monitoring observations at HartRAO restarted in 2019 September there was a 5-Jy signal which has continued to increase.

The 6.035 GHz emission has been stronger than the 6.031 GHz signal throughout the observation period. From 1994 to 2011, the spectra underwent some changes in amplitude, in particular the RCP and LCP peaks varied differently, but the overall shape of the spectra did not change significantly. However, by 2014 there were a few more

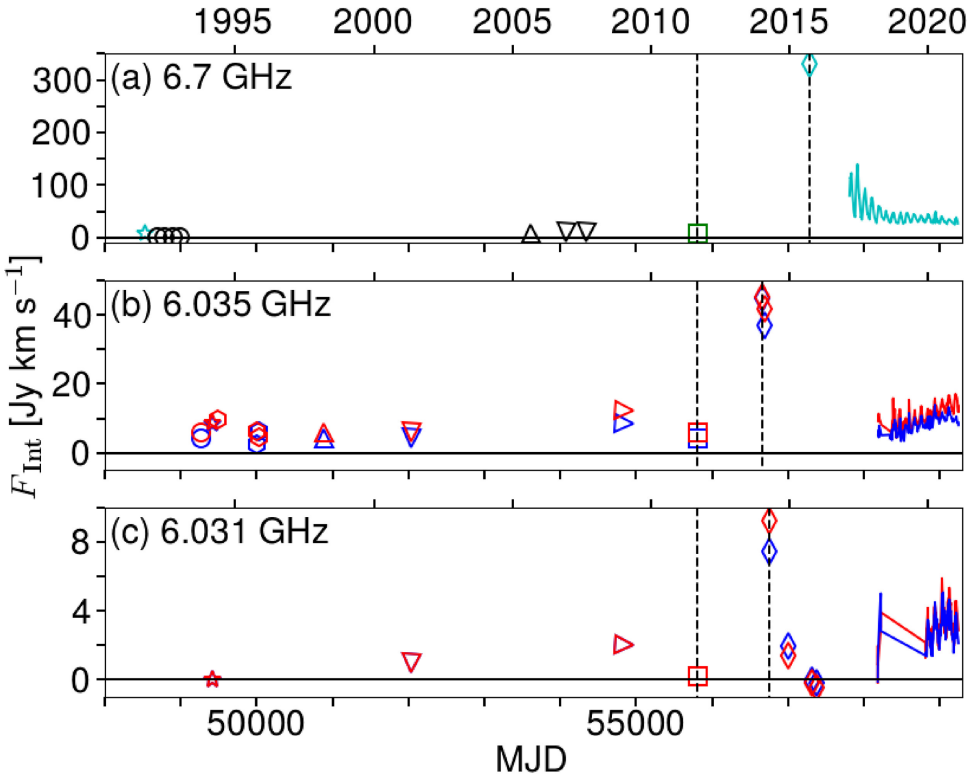

Figure 2. Time series plots of estimated or published integrated flux densities of historical observations. (a) 6.7 GHz CH_3OH observations by MacLeod et al. (1992) (cyan star), Caswell et al. (1995) (black circles), Ellingsen (2007) (black triangle), Green et al. (2012a) (black upside-down triangles), Green et al. (2015) (green square), Proven-Adzri et al. (2019) (cyan diamond), and monitoring results (cyan solid line). (b) 6.035 GHz exOH observations by Smits (1994) (stars), Smits (private communication) (hexagonals), Caswell & Vaile (1995) (circles), Caswell & Reynolds (2001) (triangles), Caswell (2003) (upside down triangles), Avison et al. (2016) (right pointing triangles), Green et al. (2015) (squares), this work (diamonds), and the monitoring data (solid lines). (c) 6.031 GHz exOH observations by Smits (1994) (stars), Caswell (2003) (upside-down triangles), Avison et al. (2016) (right-pointing triangles), Green et al. (2015) (squares), this work (diamonds), and monitoring results (solid lines). RCP observations are denoted by red symbols and lines, LCP by blue.

features in the spectrum than in the earlier spectra, and the peak flux had doubled. There was a new peak at $v = -69.5\,\mathrm{km\,s^{-1}}$ which is close to that of the dominant 6.7 GHz CH_3OH that appeared in 2015 (indicated by the dotted line in Fig. 1). There was no detectable 6.031 GHz maser emission above $3\sigma - 0.5$ Jy at this velocity. The activity at the reddest velocities ($-66\,\mathrm{km\,s^{-1}}$) in the most recent 6.035 GHz spectra has decreased and can no longer be detected above $3\sigma - 0.5$ Jy.

Between 1992 (MacLeod et al. 1992) and 2011 (Green et al. 2015) the 6.7 GHz methanol emission did not vary by more than ~ 20 per cent; the peak flux density had a range of 16−22 Jy in the velocity range from -68.5 to $-66.0\,\mathrm{km\,s^{-1}}$, peaking around $v = -67\,\mathrm{km\,s^{-1}}$.

An event appears to have occurred after 2011 that resulted in both the hydroxyl and methanol masers brightening significantly. New 6.7 GHz maser emission appeared in the velocity range from $v = -70.9$ to $-68.5\,\mathrm{km\,s^{-1}}$, with the brightest feature in the 2015 spectrum being a new line at $v = -69.35\,\mathrm{km\,s^{-1}}$. This line had a peak flux density of 504 Jy on 2015 September 24 (Proven-Adzri et al. 2019), which decayed to 9.3 Jy by 2017 February 28 and has subsequently dropped below detection limits, $3\sigma - 2.5$ Jy, at HartRAO. The strongest maser emission after 2015 was at $v = -67.1\,\mathrm{km\,s^{-1}}$ and is still stronger than the peak from the brightest maser between 1992 and 2011.

In Fig. 2, total integrated flux densities of historical observations and the monitoring data are plotted. The origin of these data is presented in the figure caption. The temporal extent inside which the onset of an accretion event may have occurred is delineated in each panel. The vertical (dashed) lines represent the observation dates for each transition constraining the flaring event. The 6.031 GHz exOH masers brightened significantly in 2014 January but declined to previous levels by the year's end and were undetectable in two epochs during 2015. The historical observations of the 6.035 GHz exOH masers provide the best constraint, between 2011 September 24 and 2014 January 8, as to when the putative accretion event occurred. No gsOH maser observations were taken within this period.

4.2 Monitoring observations

Results of monitoring five transitions are presented here. Dynamic spectra and time series of selected maser features are presented for methanol in Fig. 3. Similarly, dynamic spectra and time series of selected hydroxyl features are shown in Fig. 4. Results of analysis of all features using the techniques described in Section 3.2 are presented in Table 2. If the measured time lags are not statistically significant they are listed as upper limits equivalent to 1σ.

From the spectra, seven 6.7 GHz CH_3OH maser features are identified as being periodic. An ephemeris based on the flux density of the mean of the PP maximum features is given by

$$D(n) = 92.5 \pm 0.5 \times (n - 1) + 57828 \pm 5. \quad (1)$$

Relative to the $v = -68.13\,\mathrm{km\,s^{-1}}$ feature, only two features, $v = -69.04$ and $-68.79\,\mathrm{km\,s^{-1}}$ have no measurable time lag. Time lags estimated from minima are less accurate.

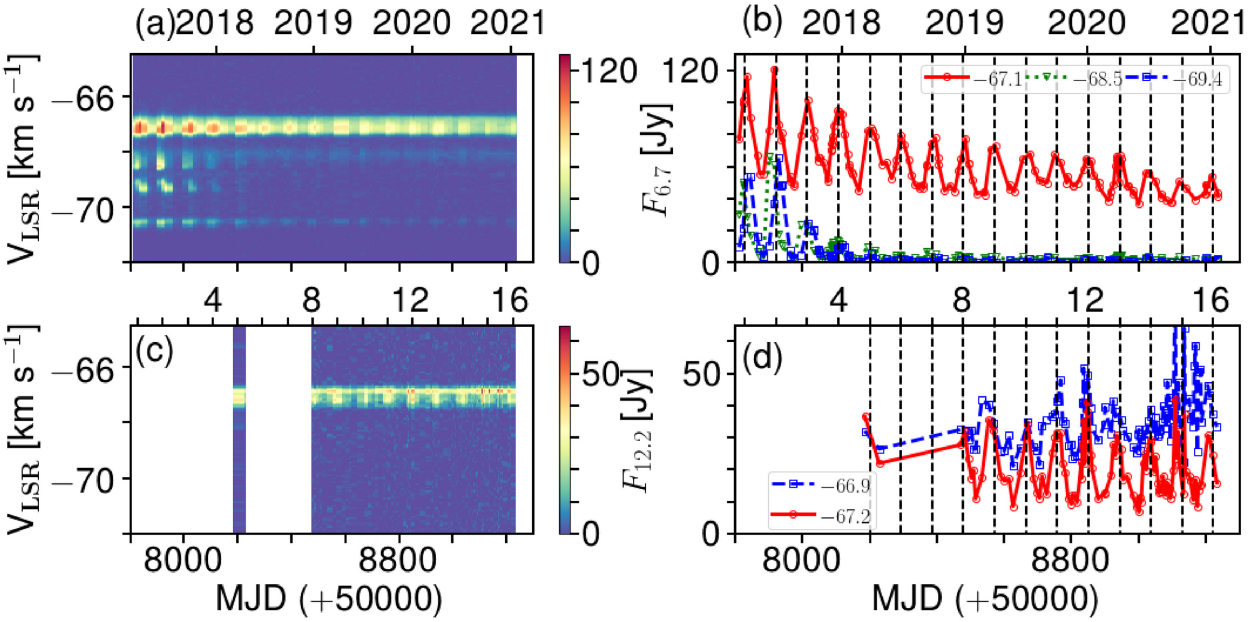

Figure 3. Results of the CH_3OH monitoring observations of G323.459–0.079: (a) 6.7 GHz dynamic spectral plot, (b) 6.7 GHz time series plots for selected velocity channels, (c) 12.2 GHz dynamic spectral plot, and (d) 12.2 GHz time series plots for selected velocity channels. The vertical dashed lines indicate the peaks of the 6.7 GHz methanol maser flares which are numbered consecutively. The upper axes on both (c) and (d) are labelled with flare numbers for $n = 1-16$.

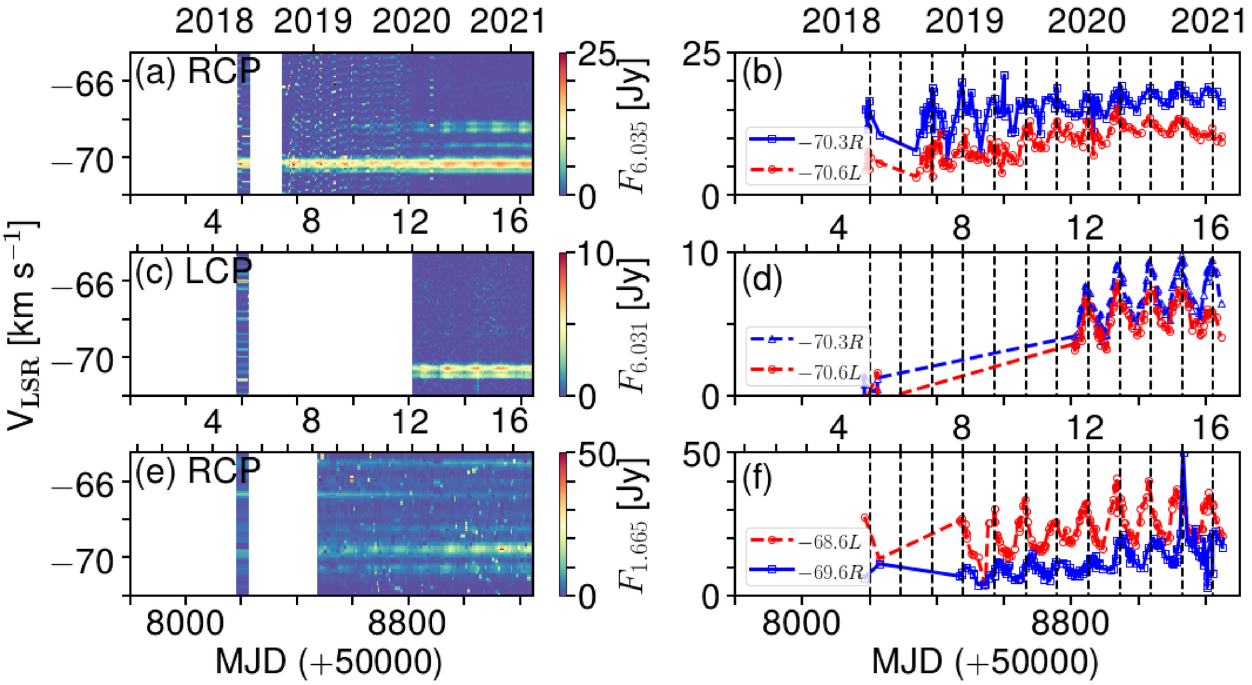

Figure 4. Results of OH monitoring observations of G323.459–0.079: (a) 6.035 GHz RCP dynamic spectral plot, (b) time series plots of selected 6.035 GHz R and LCP velocity channels, (c) 6.031 GHz LCP dynamic spectral plot, and (d) time series plots of selected 6.031 GHz R and LCP velocity channels. (e) 1.665 GHz RCP dynamic spectral plot, and (f) time series plots of selected 1.665 GHz R and LCP velocity channels. The dashed lines indicate the peaks of the periodic 6.7 GHz methanol masers with each flare numbered consecutively. The upper axes on (c), (d), (e), and (f) label flare numbers.

Two 12.2 GHz methanol maser features are varying contemporaneously with the 6.7 GHz methanol maser and have a similar period, $\tau_{PP} \sim 91$ d, but larger uncertainties (see Table 2). No time lags are found. The brighter of the two features is at $v = -66.86$ km s^{-1} and undergoes random flaring within the flare cycles, resulting in $\tau_{LS} =$ 75.7 d. For the second feature the LS and PP periods are similar within the uncertainties.

The total integrated flux density of the 6.7 GHz maser emission has been decaying since at least 2018. So too is the amplitude of the flares, which decreased from ∼100 to 25 Jy km s^{-1}. The integrated

Table 2. Information of individual periodic maser features in each transition. Included are the mean velocity of each feature, the velocity extent in which $F_{\rm Int}$ is determined, maximum $F_{\rm Int}$, period determined from the LS and PP methods, and MJD dates at which each reached their first maximum. Also included are time lags, estimated with respect to the maxima and minima of the $v = -68.13\,{\rm km\,s^{-1}}$ maser feature.

Mol.	Freq. (GHz)	Pol.	Mean velocity (km s^{-1})	Velocity extent (km s^{-1})	Flare max D_1 (MJD)	Period $\tau_{\rm LS}$ (d)	Period $\tau_{\rm PP}$ (d)	Time Lag $\Delta t_{\rm max}$ (d)	Time Lag $\Delta t_{\rm min}$ (d)
CH_3OH	6.7	R + L	–70.52(07)	0.60	57823	92.0	92(10)	+14(7)	<11
CH_3OH	6.7	R + L	–69.38(10)	0.50	57835	92.9	93(10)	+21(6)	<10
CH_3OH	6.7	R + L	–69.04(10)	0.40	57823	93.9	94(15)	<5	<7
CH_3OH	6.7	R + L	–68.79(04)	0.20	57835	93.7	93(19)	<14	<15
CH_3OH	6.7	R + L	–68.40(07)	0.40	57823	92.8	93(10)	+13(5)	<5
CH_3OH	6.7	R + L	–68.13(07)	0.50	57823	92.6	92(11)	Reference	Channel
CH_3OH	6.7	R + L	–67.17(03)	0.60	57835	92.9	93(9)	+16(3)	<10
$Ave_{6.7}$					57828(5)	93.0(6)	92.5(5)		
CH_3OH	12.2	R + L	–67.17(05)	0.75	58483	91.3	92(17)	<8	<9
CH_3OH	12.2	R + L	–66.86(01)	0.53	58470	75.7	90(22)	<15	<12
OH	6.035	R	–70.30(06)	0.67	58385	92.4	93(6)	<11	<8
OH	6.035	R	–69.57(23)	0.68	58385	92.7	93(11)	<11	<12
OH	6.035	L	–70.53(10)	0.78	58385	92.2	92(6)	<12	<8
OH	6.031	R	–70.61(04)	0.24	58842	92.0	89(10)	<25	<10
OH	6.031	R	–70.24(07)	0.63	58841	91.8	94(5)	<17	+13(5)
OH	6.031	L	–70.96(05)	0.39	58841	93.0	93(8)	<19	<10
OH	6.031	L	–70.57(04)	0.38	58841	91.6	92(11)	<14	+12(6)
OH	1.665	R	–70.55(12)	0.05	58488	91.9	91(19)	<16	–8(4)
OH	1.665	R	–69.57(06)	0.05	58484	91.1	94(14)	+19(10)	<11
OH	1.665	R	–68.50(11)	0.79	58468		92(18)	<15	<7
OH	1.665	L	–69.48(18)	0.62	58474		94(16)	<16	<14
OH	1.665	L	–68.60(08)	1.06	58475	91.2	92(15)	<15	<6

flux density of the 12.2 GHz methanol emission is more constant but the flares are becoming less developed.

Each of the hydroxyl maser transitions have periodic features. Five 1.665 GHz gsOH, four (two in each polarization) 6.031 GHz exOH, and three 6.035 GHz exOH maser features have been identified. Some 1.665 GHz gsOH and 6.031 GHz exOH features have statistically significant time lags. Significant RFI in the 1.665 GHz gsOH masers made it difficult to analyse some of the integrated flux density time series so individual velocity channels have been analysed.

An interesting result is the obvious increase of the flux density of all velocity channels shown in Fig. 4. In the 1.665 GHz dynamic spectrum features at $v = -66.68 \pm 0.13\,{\rm km\,s^{-1}}$ and $v = -66.80 \pm 0.22\,{\rm km\,s^{-1}}$ are non-periodic and weakening, perhaps diluting any increase in the measured integrated flux.

5 DISCUSSION

Historical observations presented here are too sparse to determine if the masers in this source were periodic prior to the flaring event. Observations shown here (see Fig. 1) clearly show variability in the 6.031 and 6.035 GHz masers, whereas the 6.7 GHz methanol masers appear to have been stable.

Some time between 2011 August 31 and 2014 January 8 maser flaring began in the 6.7 GHz CH_3OH and the 6.035 and 6.031 GHz exOH lines. Because there is no data between these dates it is not known whether the flares began abruptly or grew stronger over several months. Together with the flaring, new maser features appeared in the 6.7 GHz and 6.035 GHz spectra but not at 6.031 GHz. The brightest 6.7 GHz CH_3OH feature with $F = 504$ Jy occurred at $v = -69.38\,{\rm km\,s^{-1}}$. At present this feature is only detectable during a flare maximum when it has F(peak) ~ 2 Jy. New 6.035 GHz OH maser features at velocities of v(RCP) $= -69.43\,{\rm km\,s^{-1}}$ and v(LCP) $= -69.28\,{\rm km\,s^{-1}}$ appeared after the flare. If these features represent a Zeeman pair then the degaussed velocity due to a magnetic field of $B = -2.7$ mG would be v(degaussed) $= -69.36\,{\rm km\,s^{-1}}$. The new features in both transitions are at similar velocities, and both are weakening contemporaneously. Other features in the exOH spectra are increasing in flux (see Fig. 4) while the other CH_3OH features are all decreasing with time, and have not yet returned to pre-burst levels.

It can be seen in Fig. 2 that prior to 2012 $F_{\rm Int}(6.035) > F_{\rm Int}(6.7)$. At maximum (around 2015) $F_{\rm Int}(6.7) \sim 8 \times F_{\rm Int}(6.035)$ and in 2020 $F_{\rm Int}(6.7) \sim 6 \times F_{\rm Int}(6.035)$. Such an increase in this ratio is expected if $T_{\rm dust}$ increases from <100 K to >100 K (Cragg, Sobolev & Godfrey 2002). A temperature increase during the accretion event in NGC 6334I, which also led to the growth of new regions of maser activity in both CH_3OH and exOH, was reported by Hunter et al. (2017).

Three accretion events associated with high-mass star formation candidates, all of which had flaring CH_3OH masers, have been reported. They are S255 IR-NIRS3 (Caratti o Garatti et al. 2017), NGC 6334I (Hunter et al. 2017, 2018a), and G358.93–0.03 (Breen et al. 2019; MacLeod et al. 2019; Burns et al. 2020). New 4.660 and 6035 GHz masers were found in NGC 6334I by MacLeod et al. (2018). The methanol masers in S255 IR-NIRS3 (Szymczak et al. 2018) and NGC 6334I (MacLeod et al. 2018) displayed secondary flaring. The flaring in G358.93–0.03 occurred over months (a much shorter period than the others), and displayed multiple bursts.

Like the aforementioned accretion events, G323.459–0.079 has had flaring CH_3OH and exOH masers. A secondary flare is evident in the 6.031 GHz exOH masers; it was below detection limits in 2015 but is now increasing in flux. No secondary flaring has been observed in the 6.7 or 6.035 GHz masers (which might be due to limited

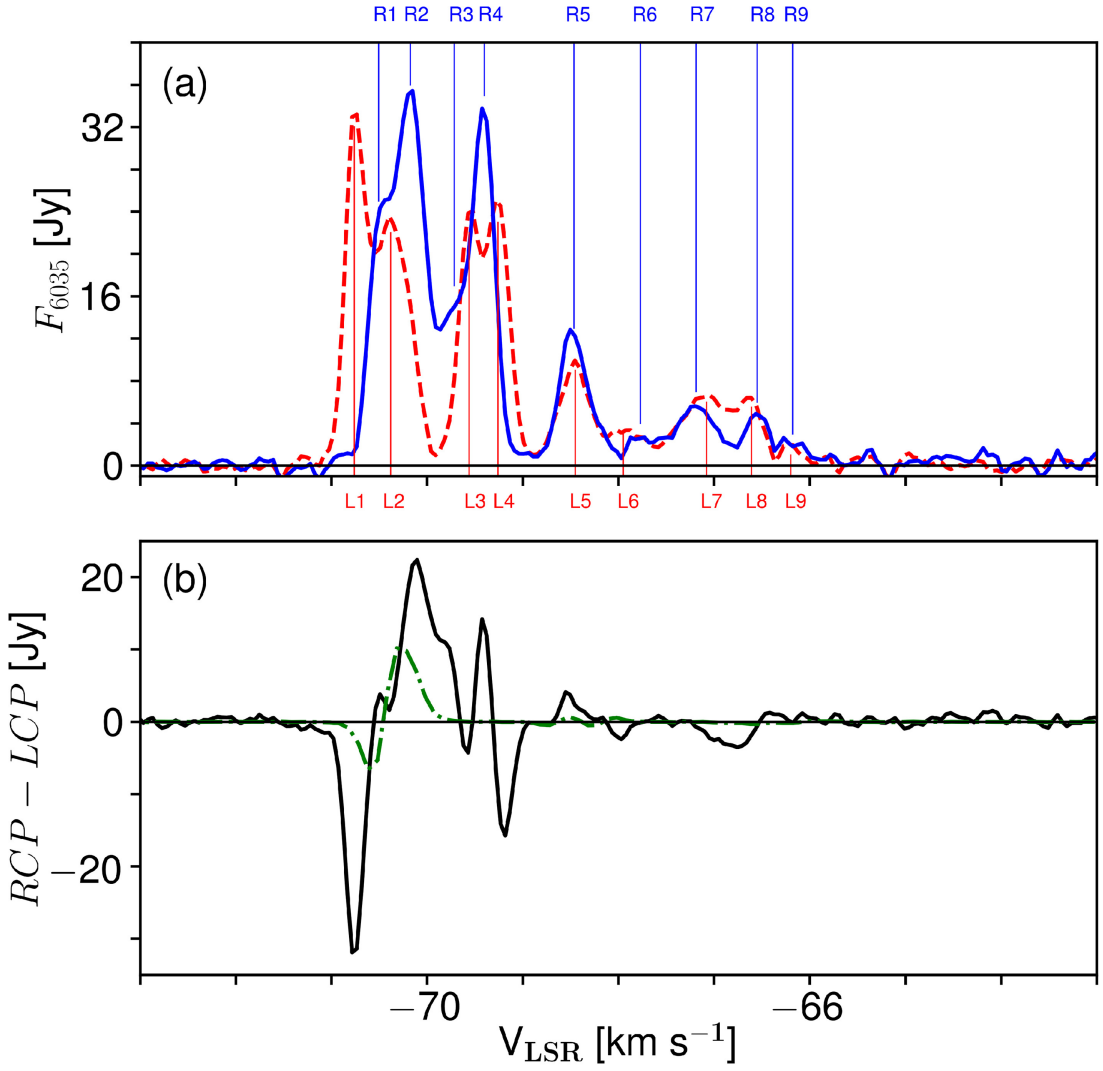

Figure 5. Plots of (a) the R (solid blue line) and LCP (dashed red line) spectra for 6.035 GHz exOH masers associated with G323.459–0.079 taken on 2014 January 8 and (b) 6.035 GHz Stokes V (RCP–LCP) (solid black line) for the same observations above. For comparison, the Stokes V spectrum from Green et al. (2015) (dot–dashed green line) is also shown. In (a) the velocity of fitted Gaussian features labelled R1–R9 and L1–L9 are marked.

monitoring of these transitions) but both transitions have new features appearing in their spectra after the flaring episode started. However, what distinguishes this event from the other accretion events is the presence of synchronized, periodic masers in multiple transitions of both CH_3OH and hydroxyl.

5.1 Magnetic field measurements

The magnetic fields of gsOH and exOH masers associated with G323.459–0.079 were reported in Caswell & Reynolds (2001) to be in the range $B = +1.47$ to $+4.13$ mG and oriented away from the observer. In Fig. 5, the RCP and LCP 6.035 GHz exOH maser spectra observed on 2014 January 8 are plotted. Nine Gaussian profiles were fitted to both spectra; when subtracted from the observed spectra the residuals were less than 1.5 Jy which is about the 3σ rms noise level. Included in this figure is the Stokes V = RCP–LCP spectrum, and that presented in Green et al. (2015). Typical Zeeman affected profiles can be seen in the lower panel. The velocity of each Gaussian profile fitted to the two spectra beginning from blueshifted to redshifted velocities are enumerated and demarcated in Fig. 5. The velocities are different from those in Table 2 as a result of line blending and variability. The results of possible Zeeman pairs for both 6.031 and 6.035 GHz exOH masers are presented in Table 3 for features nearest in velocity (Scenario 1) and a second sample of alternatives (Scenario 2 – pairs of the brightest features). Also included are the results from Green et al. (2015) for comparison purposes.

The new 6.035 GHz exOH maser feature at $v = -69.6$ km s^{-1}, may be a possible Zeeman pair labelled as R3L3 with $B = -2.7 \pm 0.4$ mG, i.e. oriented oppositely to those reported by Caswell & Reynolds (2001) and Green et al. (2015). If it is a true Zeeman pair then it may demonstrate a magnetic field reversal. Such a reversal is described in Caswell, Kramer & Reynolds (2011) for exOH masers in NGC 6334I; they report this reversal in an area unrelated to the accretion event. Several other pairs are proposed in Table 3 of which two (Z1a and R2L2 and Z4b and R9L9) compare closely to values in Green et al. (2015). The R9L9 pair has an orientation towards the observer, similar to the new feature reported here. Only a single 6.031 GHz feature appears present in Green et al. (2015) (Z2a) and observations here (R1L1) which are due to $B \sim +4$ mG. No 1.665 GHz gsOH maser Zeeman pairs were identified that matched

Table 3. Estimation of magnetic fields (B) in the 5 cm OH masers associated with G323.459–0.079. The RCP and LCP velocities and uncertainties were determined via fitting multiple Gaussian profiles. The quoted pairings are either those taken from Green et al. (2015) where the a or b denote which maser cluster they are associated with or they are our selected pairs. For $B > 0$, the orientation of the magnetic field is away from the observer.

Pairing	Trans.	Peak velocity		Degaussed velocity	Mag. field	F_ν(RCP) + F_ν(LCP)
		RCP	LCP			
	(GHz)	($\mathrm{km\,s^{-1}}$)	($\mathrm{km\,s^{-1}}$)	($\mathrm{km\,s^{-1}}$)	(mG)	(Jy)
Results of Zeeman pairs identified in Green et al. (2015) made on 2011 August 31						
Z1a	6.031	–70.18	–70.50	–70.34	+4.1 ± 0.1	0.99
Z2a	6.035	–70.28	–70.51	–70.40	+4.1 ± 0.1	22.09
Z1b	6.031	–68.39	–68.42	–68.41	+0.4 ± 0.2	0.44
Z2b	6.035	–68.49	–68.67	–68.58	+3.5 ± 0.5	3.42
Z3b	6.035	–68.08	–68.30	–68.19	+3.9 ± 0.3	3.33
Z4b	6.035	–66.04	–66.09	–66.065	+0.9 ± 0.8	1.02
6.031 GHz results of observations on 2014 April 9						
R1L1	6.031	–70.302 ± 0.003	–70.646 ± 0.005	–70.474 ± 0.008	+4.4 ± 0.1	28.4 ± 1.0
R2L2	6.031	–68.48 ± 0.02	–68.54 ± 0.04	–68.51 ± 0.06	+0.7 ± 0.7	3.0 ± 0.4
R3L3	6.031	–66.42 ± 0.03	–66.66 ± 0.05	–66.54 ± 0.08	+3.1 ± 1.0	3.6 ± 0.6
Results of observations after 2019 November 21						
R1L1 – min	6.031	–70.25 ± 0.04	–70.58 ± 0.04	–70.41 ± 0.03	+4.2 ± 1.0	
R1L1 – max	6.031	–70.54 ± 0.09	–70.96 ± 0.04	–70.75 ± 0.05	+5.3 ± 1.5	
6.035 GHz results of observations on 2014 January 8						
Scenario 1 – selected closest velocity pairs						
R1L1	6.035	–70.506 ± 0.009	–70.762 ± 0.002	–70.634 ± 0.011	+4.6 ± 0.2	43.3 ± 1.3
R2L2	6.035	–70.176 ± 0.007	–70.382 ± 0.005	–70.28 ± 0.01	+3.7 ± 0.2	51.3 ± 0.6
R3L3	6.035	–69.72 ± 0.02	–69.562 ± 0.004	–69.64 ± 0.02	–2.7 ± 0.4	22.4 ± 0.5
R4L4	6.035	–69.402 ± 0.005	–69.260 ± 0.004	–69.331 ± 0.009	–2.5 ± 0.2	53.5 ± 0.6
R5L5	6.035	–68.465 ± 0.007	–68.453 ± 0.007	–68.459 ± 0.014	–0.2 ± 0.3	19.9 ± 0.5
R6L6	6.035	–67.77 ± 0.03	–67.96 ± 0.03	–67.86 ± 0.07	+3.4 ± 1.2	7.9 ± 0.3
R7L7	6.035	–67.19 ± 0.01	–67.08 ± 0.01	–67.14 ± 0.03	–1.8 ± 0.5	12.4 ± 0.4
R8L8	6.035	–66.55 ± 0.01	–66.61 ± 0.01	–66.58 ± 0.02	+1.0 ± 0.4	7.7 ± 0.8
R9L9	6.035	–66.18 ± 0.03	–66.20 ± 0.02	–66.19 ± 0.05	+0.4 ± 0.9	3.0 ± 0.7
Results of observations after 2019 November 21						
R1L1 – min	6.035	–70.37 ± 0.06	–70.57 ± 0.04	–70.47 ± 0.04	+3.7 ± 1.4	
R1L1 – max	6.035	–70.74 ± 0.05	–70.99 ± 0.04	–70.87 ± 0.03	+4.4 ± 1.1	
R4L4 – min	6.035	–69.60 ± 0.05	–69.7 ± 0.1	–69.65 ± 0.07	–0.9 ± 3.3	
R4L4 – max	6.035	–69.36 ± 0.03	–69.39 ± 0.04	–69.37 ± 0.02	–0.5 ± 0.7	
Scenario 2 – pairs of the brightest features						
R2L1	6.035	–70.176 ± 0.007	–70.762 ± 0.002	–70.469 ± 0.009	+10.46 ± 0.08	64.6 ± 0.9
R4L3	6.035	–69.402 ± 0.005	–69.562 ± 0.004	–69.482 ± 0.009	+2.86 ± 0.03	55.2 ± 1.4
R5L4	6.035	–68.465 ± 0.007	–69.260 ± 0.004	–68.862 ± 0.011	+14.19 ± 0.05	36.9 ± 0.7

any in Caswell & Reynolds (2001). If it is assumed that the brightest features represented Zeeman pairs, then they resulted in very large magnetic fields relative to those in Green et al. (2015), see results labelled Scenario 2 in Table 3. There is no measurable magnetic field variation during the monitoring of the periodic flare cycles.

5.2 Physical distribution of the periodic masers

The increased activity seen in both methanol and hydroxyl masers in G323.459–0.079, as well as the formation of new features, indicates that a major flaring event has occurred in this object. This raises the question of where the new masers are located.

For ease of discussion, a spot map of previously detected masers towards G323.459–0.079 is presented in Fig. 6. Several interferometric observations of hydroxyl (Caswell & Reynolds 2001) and methanol (Caswell & Vaile 1995; Caswell 1997; Green et al. 2015) have been published. Maser position maps for the 1.665 GHz gsOH masers of G323.459–0.079 are shown in Caswell & Reynolds (2001). They list 14 sites of maser emission. A recreation of the maser position spot map in Caswell & Reynolds (2001) is presented in Fig. 6 in which three regions of maser activity are listed and labelled South (S), Central (C), and North (N). Only the maser region in N is at the edge of the H II region. The 6.7 GHz methanol masers are found in the S and C regions, while the 12.2 GHz methanol masers (Breen et al. 2012) were only in C. Green et al. (2015) identified four sites of exOH and CH_3OH maser activity in agreement with Caswell (1997); sites b and c comprise the region C. Several of the gsOH masers appear near regions of the exOH masers in both C and N. One methanol site (no OH emission) is situated in S, the second methanol site is in C. The gsOH and exOH masers are distributed similarly in C and N and have similar velocity extents (Caswell & Reynolds 2001). The C and N regions of maser activity are separated by ∼1 arcmin while S is about ∼0.′7 from C. At a kinematic distance of 3.8 ± 0.4 kpc (Green & McClure-Griffiths 2011) these separations are ∼3800 and ∼2850 au. The light travel times across such distances are ∼22 and 15 d, respectively.

In Fig. 6 concentric light travel times (5.5, 11, and 22 d) are plotted centred on the feature at $v = -68.13\,\mathrm{km\,s^{-1}}$. Time lags are listed in Table 2 measured against this feature. Several features in each transition were detectable in spectra taken before and after the flaring event. The periodic nature of so many features, each varying contemporaneously, in different species and transitions suggests

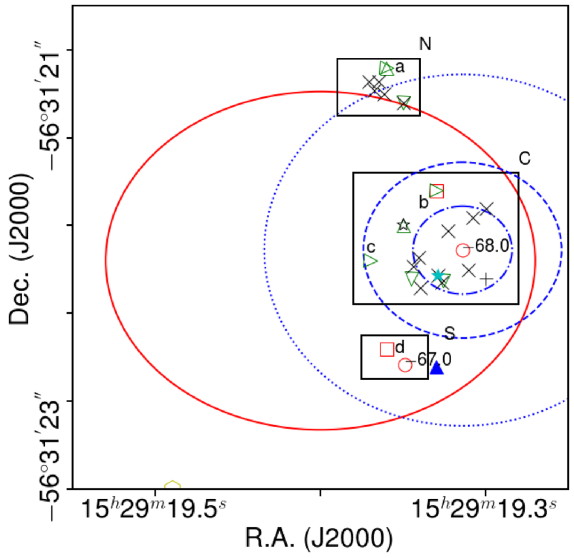

Figure 6. Maser position spot map for both OH and CH_3OH masers. Symbols representing the different maser species are labelled as follows: 1.665 GHz gsOH (black X's), 6.035 GHz exOH (green upside-down triangles), and 6.7 GHz (red circles). The 6.031 GHz exOH (green right-pointing triangles), 6.035 GHz exOH (green triangles), and 6.7 GHz CH_3OH (red squares) positions from Green et al. (2015) are also plotted. The blue filled triangle marks the position of the 12.2 GHz methanol maser reported in Breen et al. (2012). The red ellipse delineates the UCH II as presented in Caswell & Reynolds (2001). The cyan filled star identifies the 1.665 GHz gsOH maser velocity at which no periodicity is found. Regions labelled North (N), Central (C), and South (S) are demarcated by black rectangles. The positions labelled in lower case (a) through (d) from Green et al. (2015) are included. Blue circles demarcate the estimated light traveltime from the $v = -68.04\,\mathrm{km\,s^{-1}}$ position given in Caswell & Reynolds (2001) (dot–dashed are ±5.5 d, dashed are ±11 d, and dotted are ±22 d.

a common background driving source. These two results suggest that the majority of the features reside in previously identified regions of maser activity. Also, it is possible the periodic flaring propagates outward from C. Three 6.7 GHz CH_3OH features at $v = -70.52$, -69.38 and $-67.17\,\mathrm{km\,s^{-1}}$, have similar, and greater than 1σ, minimum and maximum time lags. There is either increased methanol maser activity in both C and S or a new region of maser activity has developed. The latter two features may reside in S while the first is in either N, S, or elsewhere. Less clear are the features with only a significant minimum or maximum time lag, e.g. at $v = -69.04$ or $-68.40\,\mathrm{km\,s^{-1}}$. Two 6.031 GHz features appear to activate later than the CH_3OH $v = -68.13\,\mathrm{km\,s^{-1}}$ feature. This could be because they are in a region with different conditions to where the CH_3OH maser is. It is also possible that line blending of multiple features in different areas blur out the time lags. Those with no measurable lags may simply reside in the proposed progenitor region C which contains the feature at $v = -68.13\,\mathrm{km\,s^{-1}}$. The zero time lag for the new 6.035 GHz exOH maser feature at $v = -69.6\,\mathrm{km\,s^{-1}}$ suggests it also resides in C. However, its estimated magnetic field orientation is opposite to those measured by Caswell & Reynolds (2001).

Variations of the flux densities of these masers do not resolve where these masers are located. The flux densities of excited OH and CH_3OH masers increased during the accretion event, possibly the result of an outburst from a common background proto-stellar object. After this event, the strengthening and weakening of the hydroxyl and methanol masers, respectively, may be the result of changing column densities of the respective species. This may occur whether they are co-located or not. The overlap of velocity features with similar velocities from different regions of maser activity in single-dish spectra further confound any interpretation. New interferometric observations are required to determine where these maser spots reside relative to one another, the strength and orientation of their magnetic fields, and the position of the maser spots with respect to the background radio continuum source.

6 CONCLUSIONS

The first confirmed periodically varying 6.031 and 6.035 GHz exOH masers are reported here in the source G323.459–0.079. The 1.665 GHz OH and 12.2 GHz CH_3OH masers associated with this source are also periodic. All these masers vary contemporaneously with the 6.7 GHz CH_3OH masers in G323.459–0.079. Periodicity is seen in all masers reported here except for a single 1.665 GHz OH maser feature. These observations, together with historical published results, suggest a possible accretion event occurred between 2011 August 31 and 2014 January 8. It is proposed that the increased maser activity at all observed transitions is in regions S and C (see Fig. 6). The fluxes of the 6.7 GHz methanol masers have subsided significantly since the flaring began, while both the periodic gsOH and exOH masers are increasing. Insufficient observations were taken historically to determine whether periodicity was present prior to the putative accretion event. A simple explanation of the time lags is radiation propagating outward from region C.

Analysis of the possible Zeeman effect seen in the 6.035 GHz exOH maser emission produced an interesting result. Possible Zeeman pairs are determined associated with this source with two scenarios, and in one it is seen that the source may exhibit a field reversal as a result of the accretion event.

Monitoring of the 1.665, 6.031, and 6.035 GHz OH, 6.7 and 12.2 GHz CH_3OH masers, and 22.2 GHz H_2O masers associated with G323.459–0.079 continues. Interferometric observations are required for all maser transitions (1) to confirm if a new region of maser activity has been activated, (2) to determine where the periodic features reside, and (3) the nature of the polarization of the regions.

ACKNOWLEDGEMENTS

We thank Dr. Jonathan Quick for his ongoing efforts to schedule time around various other observing programmes at HartRAO. We would also like to thank the Maser Monitoring Organization (M2O) for support, in particular Dr. Bringfried Stecklum for fruitful discussions. The Hartebeesthoek 26-m telescope is operated by the South African Radio Astronomy Observatory, which is a facility of the National Research Foundation, an agency of the Department of Science and Innovation.

DATA AVAILABILITY

The data underlying this article were accessed from the Hartebeesthoek Radio Astronomy Observatory. Public domain access is being developed but not yet available. The data used in this research will be shared on reasonable request to G. MacLeod.

REFERENCES

Araya E. D., Hofner P., Goss W. M., Kurtz S., Richards A. M. S., Linz H., Olmi L., Sewiło M., 2010, ApJ, 717, L133
Avison A. et al., 2016, MNRAS, 461, 136

Breen S. L., Ellingsen S. P., Caswell J. L., Green J. A., Voronkov M. A., Fuller G. A., Quinn L. J., Avison A., 2012, MNRAS, 426, 2189
Breen S. L., Sobolev A. M., Kaczmarek J. F., Ellingsen S. P., McCarthy T. P., Voronkov M. A., 2019, ApJ, 876, L25
Burns R. A. et al., 2020, Nat. Astron., 4, 506
Caratti o Garatti A. et al., 2017, Nat. Phys., 13, 276
Caswell J. L., 1997, MNRAS, 289, 203
Caswell J. L., 2003, MNRAS, 341, 551
Caswell J. L., Haynes R. F., 1987, Aust. J. Phys., 40, 215
Caswell J. L., Reynolds J. E., 2001, MNRAS, 325, 1346
Caswell J. L., Vaile R. A., 1995, MNRAS, 273, 328
Caswell J. L., Batchelor R. A., Forster J. R., Wellington K. J., 1989, Aust. J. Phys., 42, 331
Caswell J. L., Vaile R. A., Ellingsen S. P., Whiteoak J. B., Norris R. P., 1995, MNRAS, 272, 96
Caswell J. L., Kramer B. H., Reynolds J. E., 2011, MNRAS, 414, 1914
Cohen R. J., Baart E. E., Jonas J. L., 1988, MNRAS, 231, 205
Cragg D. M., Sobolev A. M., Godfrey P. D., 2002, MNRAS, 331, 521
Ellingsen S. P., 2007, MNRAS, 377, 571
Goedhart S., Gaylard M. J., van der Walt D. J., 2003, MNRAS, 339, L33
Goedhart S., Gaylard M. J., van der Walt D. J., 2004, MNRAS, 355, 553
Goedhart S., Langa M. C., Gaylard M. J., Van Der Walt D. J., 2009, MNRAS, 398, 995
Green J. A., McClure-Griffiths N. M., 2011, MNRAS, 417, 2500
Green J. A. et al., 2012a, MNRAS, 420, 3108
Green J. A., Caswell J. L., Voronkov M. A., McClure-Griffiths N. M., 2012b, MNRAS, 425, 1504
Green J. A., Caswell J. L., McClure-Griffiths N. M., 2015, MNRAS, 451, 74
Hamaker J. P., Bregman J. D., 1996, A&AS, 117, 161
Hunter T. R. et al., 2017, ApJ, 837, L29
Hunter T. R., Brogan C. L., Chibueze J. O., Cyganowski C. J., Hirota T., MacLeod G. C., 2018a, in Tarchi A., Reid M. J., Castangia P., eds, Proc. IAU Symp. 336, Astrophysical Masers: Unlocking the Mysteries of the Universe. Kluwer, Dordrecht, p. 251
Hunter T. R. et al., 2018b, ApJ, 854, 170
Kemball A. J., Gaylard M. J., Nicolson G. D., 1988, ApJ, 331, L37
MacLeod G. C., Gaylard M. J., Nicolson G. D., 1992, MNRAS, 254, 1P
MacLeod G. C. et al., 2018, MNRAS, 478, 1077
MacLeod G. C. et al., 2019, MNRAS, 489, 3981
MacLeod G. C., Chibueze J. O., Sanna A., Paulsen J. D., Houde M., van den Heever S. P., Goedhart S., 2020, MNRAS, 500, 3425
Maswanganye J. P., Gaylard M. J., Goedhart S., Walt D. J. v. d., Booth R. S., 2015, MNRAS, 446, 2730
Maswanganye J. P., van der Walt D. J., Goedhart S., Gaylard M. J., 2016, MNRAS, 456, 4335
Mottram J. C., Hoare M. G., Lumsden S. L., Oudmaijer R. D., Urquhart J. S., Sheret T. L., Clarke A. J., Allsopp J., 2007, A&A, 476, 1019
Olech M., Szymczak M., Wolak P., Gérard E., Bartkiewicz A., 2020, A&A, 634, A41
Ott M., Witzel A., Quirrenbach A., Krichbaum T. P., Standke K. J., Schalinski C. J., Hummel C. A., 1994, A&A, 284, 331
Parfenov S. Y., Sobolev A. M., 2014, MNRAS, 444, 620
Proven-Adzri E., MacLeod G. C., Heever S. P. v. d., Hoare M. G., Kuditcher A., Goedhart S., 2019, MNRAS, 487, 2407
Sanna A. et al., 2015, ApJ, 804, L2
Scargle J. D., 1982, ApJ, 263, 835
Smits D. P., 1994, MNRAS, 269, L11
Sugiyama K. et al., 2017, PASJ, 69, 59
Szymczak M., Wolak P., Bartkiewicz A., van Langevelde H. J., 2011, A&A, 531, L3
Szymczak M., Wolak P., Bartkiewicz A., 2015, MNRAS, 448, 2284
Szymczak M., Olech M., Wolak P., Bartkiewicz A., Gawroński M., 2016, MNRAS, 459, L56
Szymczak M., Olech M., Wolak P., Gérard E., Bartkiewicz A., 2018, A&A, 617, A80
van der Walt D. J., Maswanganye J. P., Etoka S., Goedhart S., van den Heever S. P., 2016, A&A, 588, A47
Walsh A. J., Burton M. G., Hyland A. R., Robinson G., 1998, MNRAS, 301, 640

This paper has been typeset from a TEX/LATEX file prepared by the author.